Theor Appl Climatol (2018) 132:313–326
DOI 10.1007/s00704-017-2085-x

ORIGINAL PAPER

Variability in rainfall over tropical Australia during summer and relationships with the Bilybara High

C. J. C. Reason [1]

Received: 1 September 2016 / Accepted: 15 February 2017 / Published online: 6 March 2017

Abstract Variability in summer rainfall over tropical Australia, defined here as that part of the continent north of 25° S, and its linkages with regional circulation are examined. In particular, relationships with the mid-level anticyclone (termed the Bilybara High) that exists over the northwestern Australia/Timor Sea region between August and April are considered. This High forms to the southwest of the upper-level anticyclone via a balance between the upper-level divergence over the region of tropical precipitation maximum and planetary vorticity advection and moves south and strengthens during the spring and summer. It is shown that variations in the strength and position of the Bilybara High are related to anomalies in precipitation and temperature over large parts of tropical Australia as well as some areas in the south and southeast of the landmass. Some of the interannual variations in the High are related to ENSO, but there are also a number of neutral years with large anomalies in the High and hence in rainfall. On decadal time scales, a strong relationship exists between the leading mode of tropical Australian rainfall and the Bilybara High. On both interannual and decadal scales, the relationships between the High and the regional rainfall involve changes in the monsoonal northwesterlies blowing towards northern Australia, and further south, in the easterly trade winds over the region.

✉ C. J. C. Reason
chris.reason@uct.ac.za

[1] Department of Oceanography, University of Cape Town, Cape Town, South Africa

1 Introduction

Northern Australia, defined here as that part of the continent north of 25° S, has a tropical wet-dry climate with the austral winter half of the year being essentially dry. Typically, the summer rainy season starts sometime between September and December and lasts until March or April (Suppiah and Hennessy 1996). Most of the region receives about 75% or more of its annual mean rainfall during the 6 months of November through to April (Ropelewski and Halpert 1987; Ropelewski 1989). The summer rainfall mainly results from active phases of the monsoon and associated monsoon depressions, tropical cyclones and organised (mesoscale convective systems) and random local thunderstorms. The latter may develop within easterly troughs that typically exist in summer inland of the northwestern coast (the Pilbara Low) and over western Queensland (the Cloncurry Low).

The far north of Australia, around Darwin, and also the northern part of the Cape York Peninsula, has a monsoonal climate. However, the onset of the summer rainy season over northern Australia typically occurs earlier than the onset of the monsoon itself which has a mean onset date in late December (Drosdowsky 1996) but may be as early as mid-November or as late as mid-January (Godfred-Spenning and Reason 2002). Onset of the monsoon implies large-scale changes in regional wind and pressure, including an initial burst of northwesterly winds throughout the lower to mid-troposphere, in addition to substantial rainfall. Although most of the annual rainfall in the monsoonal region occurs during the monsoon season, both this region and the tropical region further south can receive substantial rainfall before or after it. For example, Cook and Heerdegen (2001) indicated that up to about 30% of the summer total could come from pre-monsoonal rainfall.

In this study, focus is placed on tropical Australian rainfall during the late summer (January to March) since there is

interest in exploring relationships with an aspect of the regional circulation that has not been much studied to date. This feature is the mid-level anticyclone, which exists over northwestern Australia and the Timor Sea during the summer half of the year, termed the Bilybara High, and which has counterparts over tropical southern Africa and South America (Reason 2016).

National Centers for Atmospheric Prediction (NCEP) reanalysis data (Kalnay et al. 1996) are used to examine variability in the Bilybara High and the broader-scale circulation over the Australian region during the late austral summer (January-March (JFM)), the season focussed on here. GPCC precipitation data (Schneider et al. 2008), available at a horizontal resolution of 0.5°, are used to analyse rainfall variability over Australia with a focus on the tropical region, which is that part of the continent north of 25° S. Sea surface temperature (SST) variability is assessed using the NOAA extended reconstructed dataset (Smith and Reynolds 2004). Empirical orthogonal function (EOF) analyses are applied towards understanding the nature of the interannual and interdecadal variability in tropical Australian rainfall and regional circulation with correlation and compositing analyses used to investigate the potential relationships between them.

2 Results

Figure 1 shows the leading two modes of tropical Australian rainfall variability during the summer and their associated principal components. EOF1, which explains 31% of the variance and is positive everywhere, has strongest loadings on the central Queensland coast extending inland to the Gulf of Carpentaria and the region around Darwin and weakest loadings in the Pilbara and nearby coast of Western Australia. The associated principal component PC1 (Fig. 1b) shows considerable interannual variability and is correlated at $r = -0.35$ with the Niño 3.4 index (significant at 99%), although only three of the years with the strongest five positive (negative) loadings correspond to La Niña (El Niño). Similar correlation magnitudes (0.3–0.4) between the rainfall over tropical Australia and the Southern Oscillation Index were found by Risbey et al. (2009). The largest values in Fig. 1b occur during the 1975 and 2011 La Niña summers when much of northern Australia was anomalously wet. A weaker relationship ($r = -0.30$ significant at 95%) is evident with the South Indian Ocean subtropical dipole (Behera and Yamagata 2001) whereas the correlation with the Indian Ocean Dipole is much smaller ($r = 0.13$) since this mode tends to decay after November. Another mode of climate variability that exists in the region and which influences Australia, particularly the western part of the continent, is the Ningaloo Niño (Feng et al. 2013; Kataoka et al. 2014; Tozuka et al. 2014). This mode evolves in the Leeuwin Current region off the west coast of Australia and can be

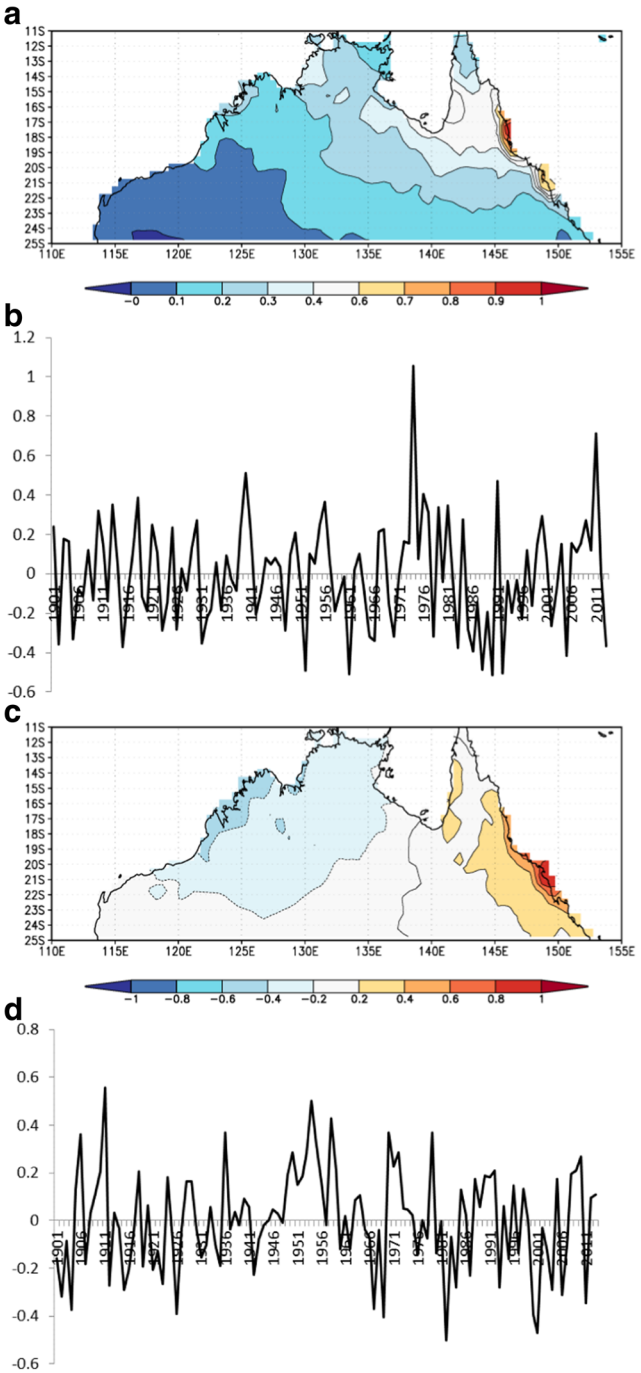

Fig. 1 Leading modes of tropical Australian JFM rainfall computed from GPCC data for 1901–2013. Panels a) and c) show EOFs 1 and 2 while b) and d) show the corresponding PCs

defined through the standardised anomaly in SST averaged between 22° and 28° S 108° E and the coast (Kataoka et al. 2014). However, the correlation between this Ningaloo Niño index and PC1 is essentially zero ($r = 0.01$).

The spatial gradient from the north towards the southwest of the domain suggests that EOF1 may be related to changes in the monsoon trough that lies over northern Australia in summer. Regressing the principal component onto the

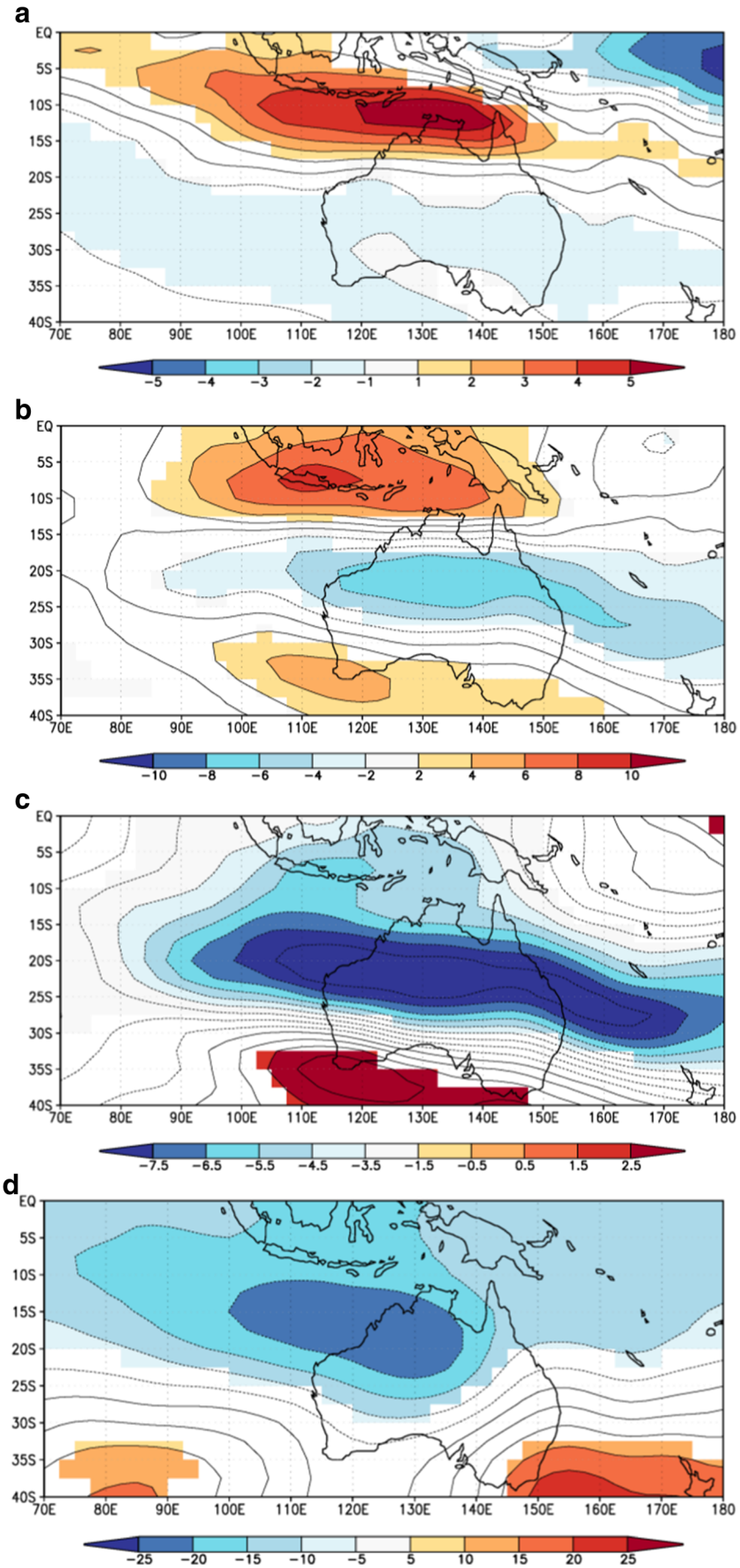

Fig. 2 Regression maps between PC1 of tropical Australian rainfall, as shown in Fig. 1b, and **a** 850 hPa zonal wind, **b** wind shear between 500 and 200 hPa levels, **c** 200 hPa zonal wind and **d** 500 hPa geopotential height computed from NCEP reanalyses for JFM

850 hPa zonal wind (Fig. 2a) and the mid- to upper-level wind shear (Fig. 2b) from NCEP reanalyses for 1948–2016 suggests that this mode is related to a strengthening of the monsoonal westerlies over the eastern equatorial South Indian Ocean and northern Australia. There is also a weaker strengthening of the easterly trade winds over the tropical South Indian Ocean, extending east over Australia to the northern Tasman Sea. Such a pattern is consistent with the monsoon trough strengthening and shifting south during summers when the first rainfall mode is strongly positive (wetter conditions throughout tropical Australia but particularly over Queensland and the Northern Territory). At 200 hPa (Fig. 2c), the regressed zonal wind shows stronger easterlies over tropical Australia and westerlies south of about 35° S, implying a southward shifted monsoon and local Hadley circulation. At 500 hPa, the regression map for geopotential height (Fig. 2d) picks out the mid-level anticyclone that typically occurs over northwestern Australia and the eastern tropical South Indian Ocean from about August until April, the Bilybara High (Reason 2016).

The second rainfall mode (Fig. 1c), which explains 16% of the variance, shows a dipole pattern with strongest positive (negative) loadings over central and southern coastal Queensland and adjacent interior (the Kimberly coast of northwestern Australia). It is not related to the El Niño-Southern Oscillation (ENSO), the IOD or the Ningaloo Niño (r = 0.01, 0.08, −0.08, respectively) and is weakly correlated with the subtropical dipole (r = −0.22). Its PC (Fig. 1d) also displays substantial interannual variability as well as periods of several years with the same sign anomaly such as during the late 1940s to mid-1950s, the early 1970s and the late 1980s to early 1990s. Like the first rainfall mode, there are changes in the monsoonal westerlies to the north and easterly trades over the South Indian Ocean and the Coral Sea (Fig. 3a); however, these wind changes are weaker and less spatially extensive. Regression of the rainfall PC2 onto the 500 hPa geopotential height (Fig. 3b) again picks out the Bilybara High as well as an opposite signed anomaly over southeastern Australia consistent with the opposite signed loadings either side of tropical Australia in this second rainfall pattern (Fig. 1c). These

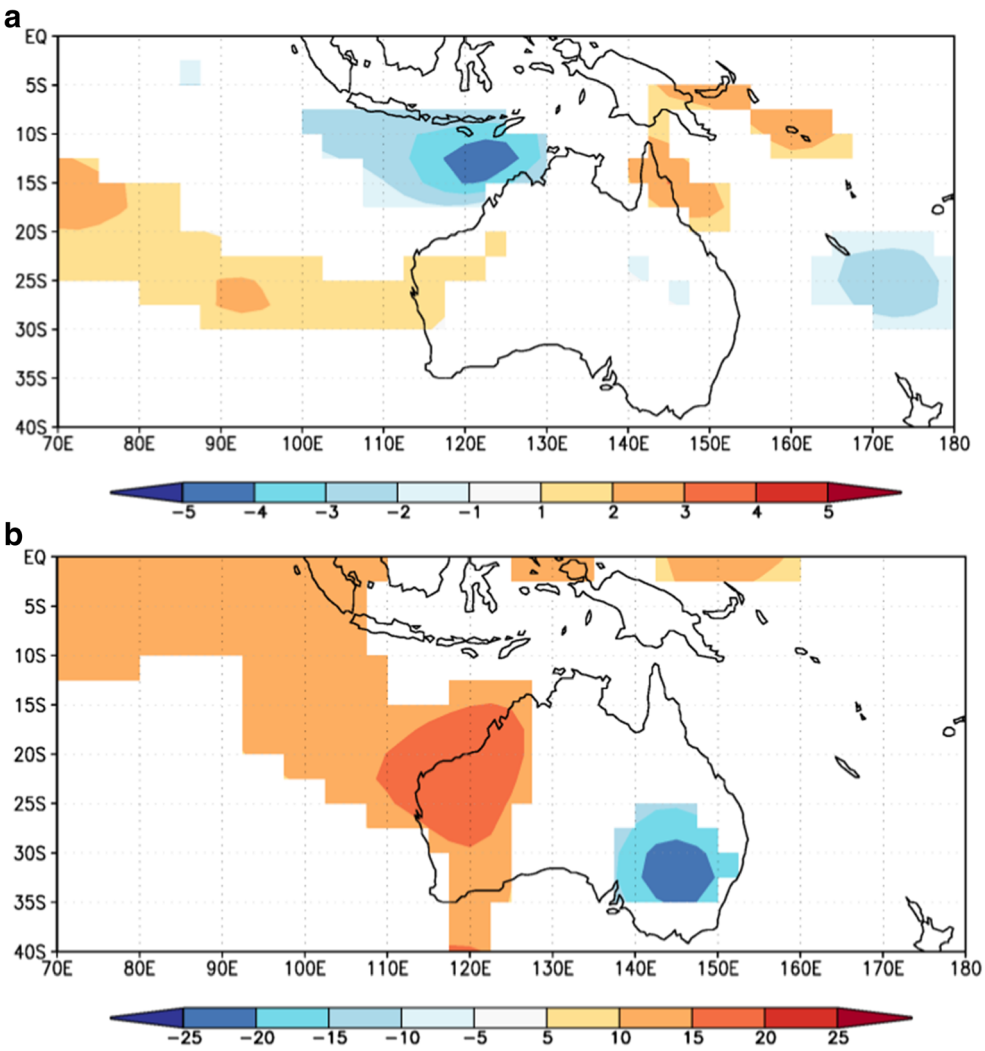

Fig. 3 Regression map of second mode of tropical Australian rainfall (shown in Fig. 1d) and **a** 850 hPa zonal wind and **b** 500 hPa geopotential height computed from NCEP reanalyses for JFM

patterns imply that increased (decreased) rainfall over coastal Queensland and adjacent interior (northwestern Australia) can be associated with decreased monsoonal westerlies towards the northwest coast, increased northwesterlies over northeast Queensland and, further south over the Coral Sea, increased easterlies. Associated with these low-level wind changes are a northward shifted and stronger Bilybara High together with a cyclonic anomaly over eastern Australia.

Figures 2d and 3b suggest that a relationship exists between the leading modes of tropical Australian summer rainfall and the mid-level anticyclone that exists over northwestern Australia during summer. Thus, variations in this Bilybara High seem important for summer rainfall over large parts of northern Australia. In order to further assess how the Bilybara High may be related to tropical Australian rainfall patterns, its annual cycle and then its other modes of variability are examined below.

2.1 Annual cycle of the Bilybara High

In the NCEP reanalysis, a weak Bilybara High is first evident in August (Fig. 4a) but its magnitude is far less than the corresponding mid-level anticyclone over southern Africa, the Botswana High (Reason 2016). Its centre is near 12° S over the Timor Sea. During the spring, the Bilybara High slowly moves southward so that by October it is centred near 14° S (Fig. 4b). However, its magnitude is only very slightly greater than in August unlike for the Botswana High whose spring time strengthening is much more evident. A more noticeable southward shift is apparent over the next 2 months with the Bilybara High now centred near 18° S just west of the northern coast of Western Australia in December (Fig. 4c). In January, the High moves onshore and further south, being centred near 23° S 125° E and has noticeably increased in magnitude. February (Fig. 4d) is the month of greatest intensity of the Bilybara High as well as its furthest southward extent; its centre is now near 25° S 125° E. During the following month, the High retreats northwestward to be located at a similar average position to January but of slightly stronger magnitude. In April, the High moves substantially northwards to again be centred north of Western Australia and over the Timor Sea at a central latitude near 16° S. Unlike the Botswana High, its magnitude has not obviously decreased from its summer maximum. The Bilybara High is no longer clearly evident in May as is also the case for the Botswana High. In general, however, the Bilybara High is weaker than the Botswana High (except in April) and shows a smaller southward shift in its centre during spring and summer.

The evolution of the Bilybara High from August to March essentially tracks that of the upper-level anticyclone at 200 hPa (not shown) except that the High is located to its southwest consistent with it forming from a balance between the upper-level divergence over the tropical high-precipitation

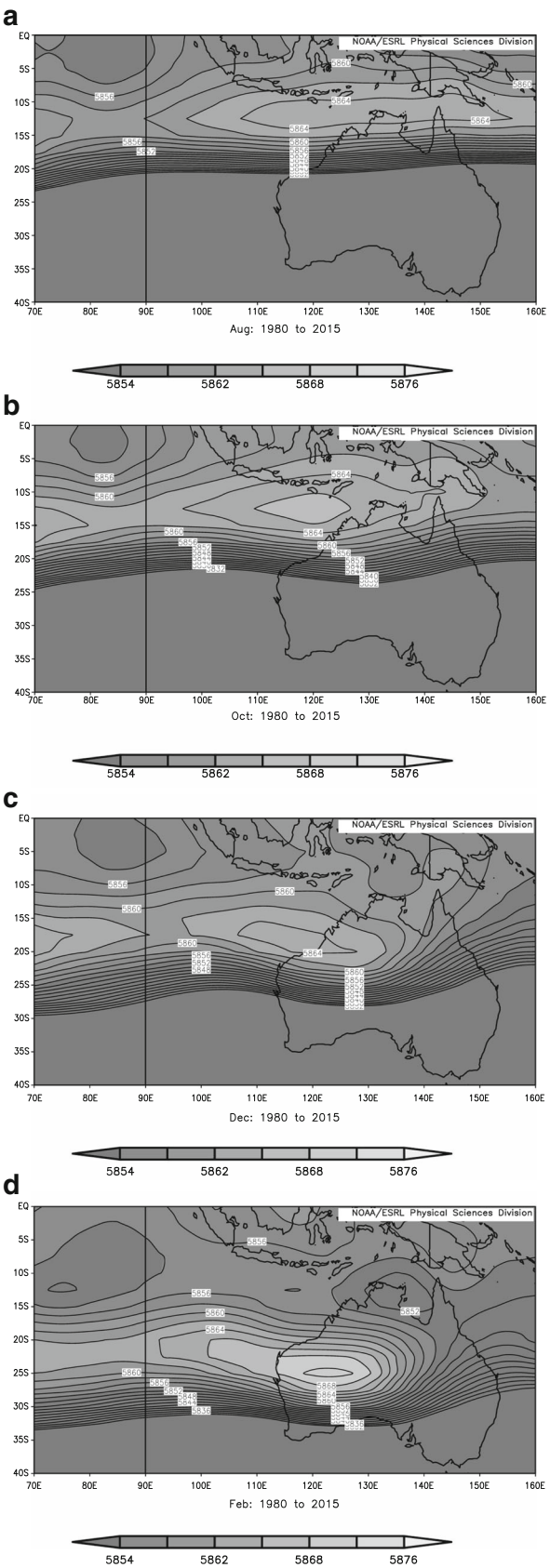

Fig. 4 Mean 500 hPa geopotential height (m) for **a** August, **b** October, **c** December and **d** February

regions and the planetary vorticity advection. This balance then implies equatorward flow to the south of the divergence maximum and high pressure to the west (Lenters and Cook 1997). The northern edge of the High is close to the region of minimum wind shear (850 hPa minus 200 hPa) (not shown) with the 0 ms^{-1} contour roughly marking the monsoon shear line over northern Australia. During the mature phase of the monsoon, there tends to be a continuous shear line right across tropical northern Australia (Davidson et al. 1983) whereas in November through to about mid-December, before the onset

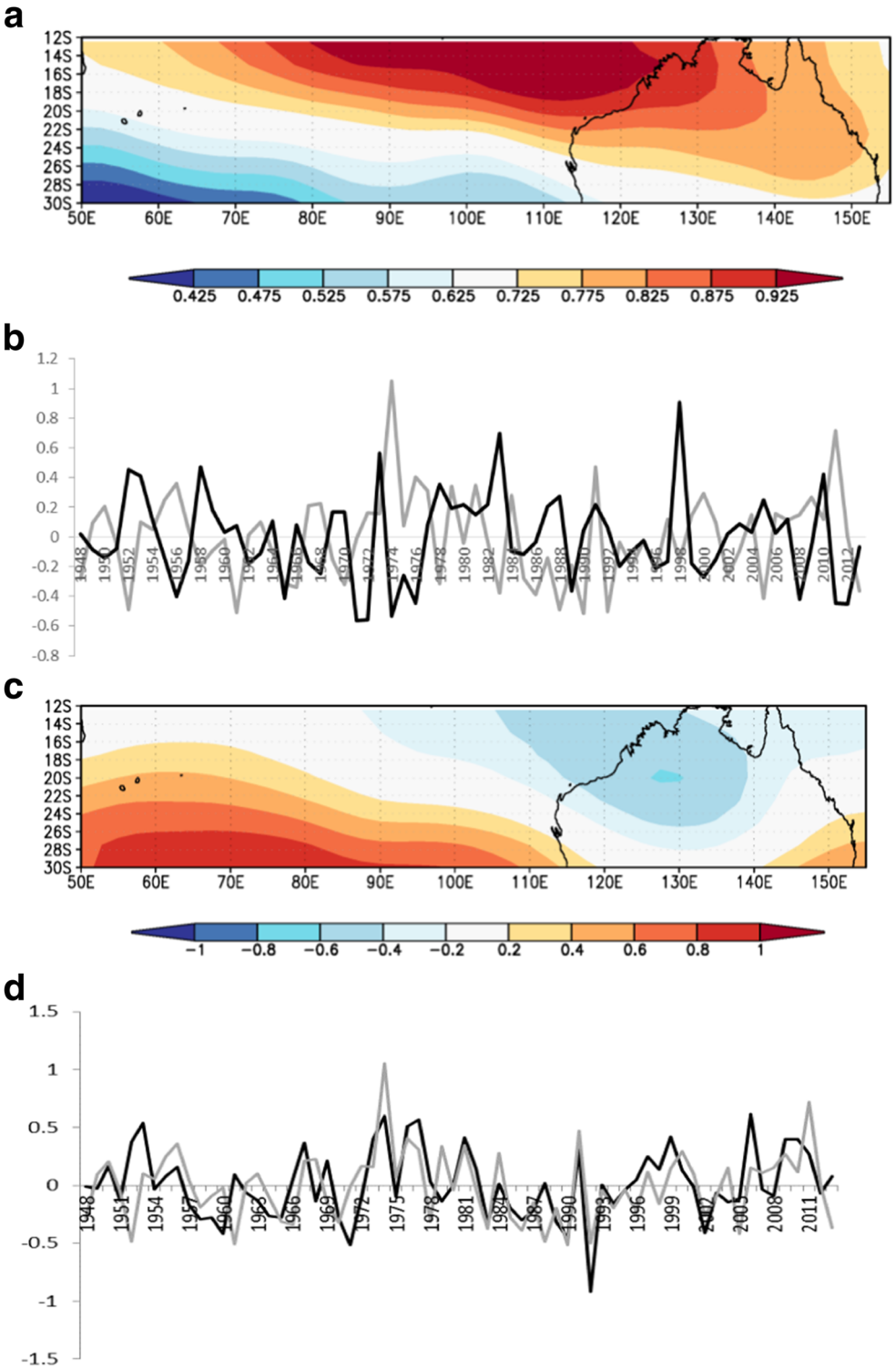

Fig. 5 EOF1 of 500 hPa geopotential height. **a**, **b** Corresponding PC1 time series (*black line*) and tropical Australia precipitation PC1 (*grey line*). **c** EOF2 of 500 hPa geopotential height. **d** Corresponding PC2 time series (*black line*) and tropical Australia precipitation PC1 (*grey line*) for JFM. The rainfall and PC1 series are correlated at **a** $r = -0.42$ (significant at 99%) while the rainfall and PC2 series are correlated at $r = 0.56$ (significant at 99.9%)

of deep westerlies that mark the beginning of the monsoon, the shear line tends to only exist over northwestern Australia and is associated with a near-surface heat low (Leslie 1980).

2.2 Interannual variability in the Bilybara High

To consider variability in the Bilybara High, Fig. 5a shows the leading mode of the JFM 500 hPa geopotential height over the South Indian Ocean/tropical Australian domain which explains 72% of the variance. EOF2 which explains 9% of the variance also shows a Bilybara High type pattern (Fig. 5c). Both EOF1 and EOF2 clearly reflect changes in the position and strength of the Bilybara High. EOFs 3 and 4 each explain only 3% of the variance and so can be considered separate from EOF2 and are not considered. The first mode is strongly related to ENSO ($r = 0.82$, significant at 99.9%) whereas the second mode is only weakly linked with ENSO ($r = -0.23$). Both these modes have a relatively weak relationship with the South Indian Ocean subtropical dipole with their respective correlation coefficients being $r = -0.22$ and $r = 0.34$ while

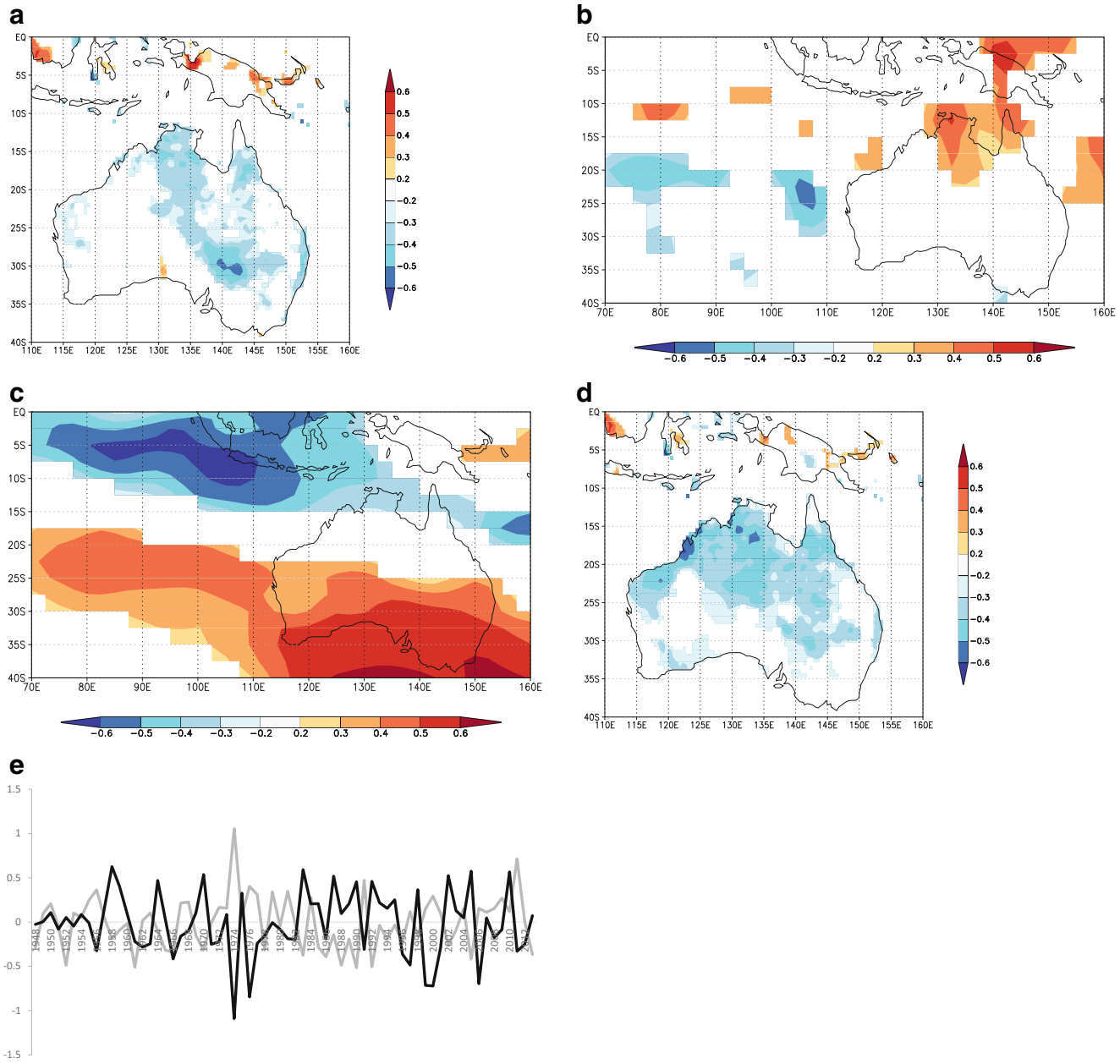

Fig. 6 Correlation between PC1 of 500 hPa geopotential height and **a** precipitation, **b** vertical velocity at 500 hPa and **c** zonal wind at 850 hPa for JFM. **d** Correlation between PC1 of precipitation and an index of 500 hPa geopotential height formed from the difference between that averaged over 110°–115° E 10°–15° S and 50°–60° E 25°–35° S. **e** Time series of this precipitation PC1 (*grey*) and the 500 hPa index (*black*). The two series are correlated at $r = -0.56$ (99% significant)

only mode one has a relationship with the Ningaloo Niño ($r = -0.35$, significant at 95%; the correlation for mode two is $r = 0.01$). However, the two Bilybara High modes are more strongly related to the leading tropical Australian rainfall pattern shown in Fig. 1a (they are correlated at −0.42 and 0.56 both significant at 99%) supporting the suggestion that this pattern of rainfall variability is linked with changes in the Bilybara High and the Australian monsoon.

EOF1 reflects a Bilybara High that has shifted northwest from its mean JFM position. Its spatial correlation with rainfall (Fig. 6a) is negative over large areas of tropical and eastern Australia with greatest values over the Northern Territory, western New South Wales and northern Queensland. The areas of rainfall change over northern Australia more or less match up with those in mid-level vertical velocity (Fig. 6b). Thus, when the High is shifted to its northwest and is stronger than average (corresponding to strong positive values in PC1 shown in Fig. 1b), weaker monsoonal northwesterlies (Fig. 6c) occur over the Timor Sea and the far north of Australia with decreased mid-level uplift (Fig. 6b), leading to decreased rainfall. At the same time, there are reduced easterlies over the Tasman Sea (Fig. 6c) leading to less transport of relatively moist marine air towards New South Wales and hence drier conditions in southeastern Australia. Such drier

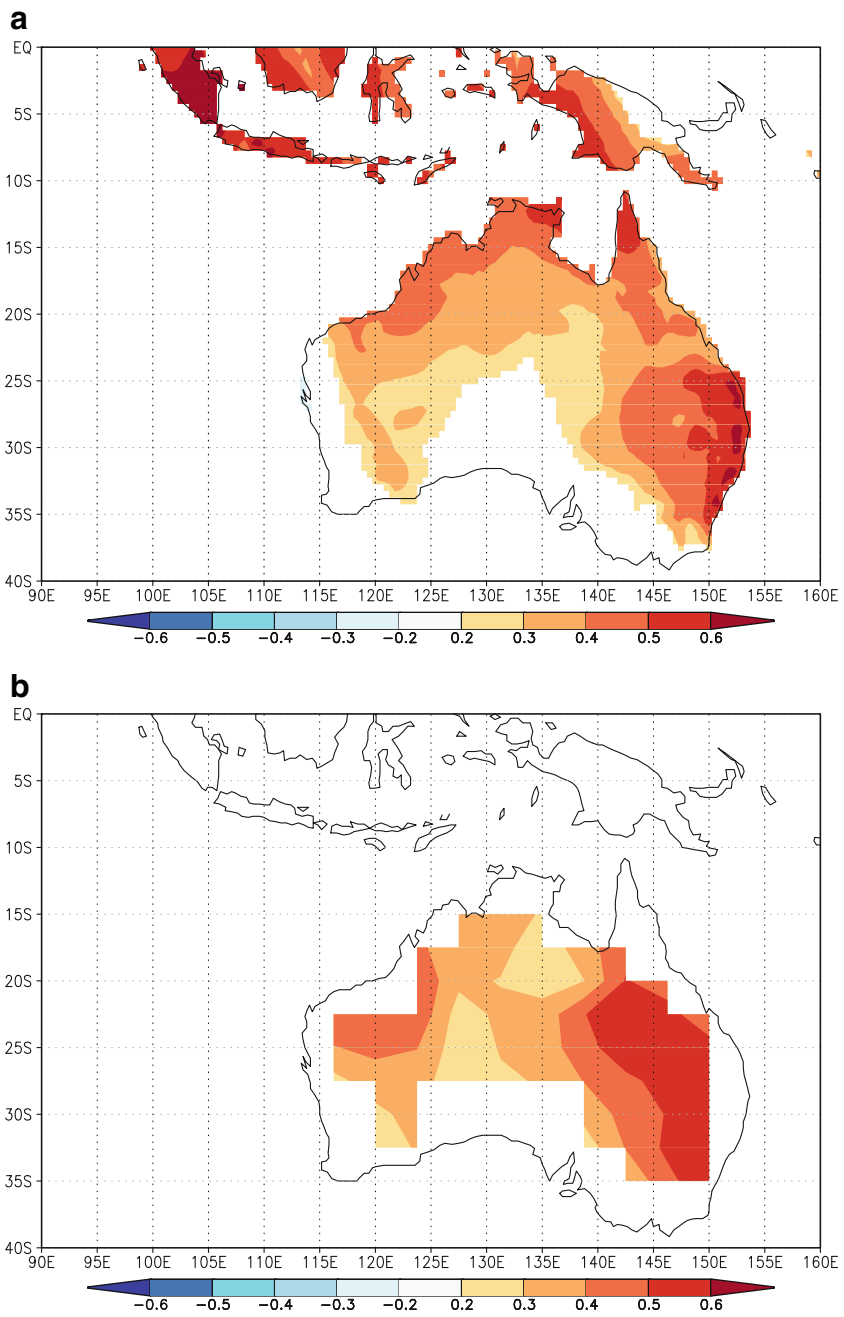

Fig. 7 Correlation between PC1 of 500 hPa geopotential height and **a** maximum surface air temperature and **b** number of days exceeding 90th percentile in surface air temperature for JFM

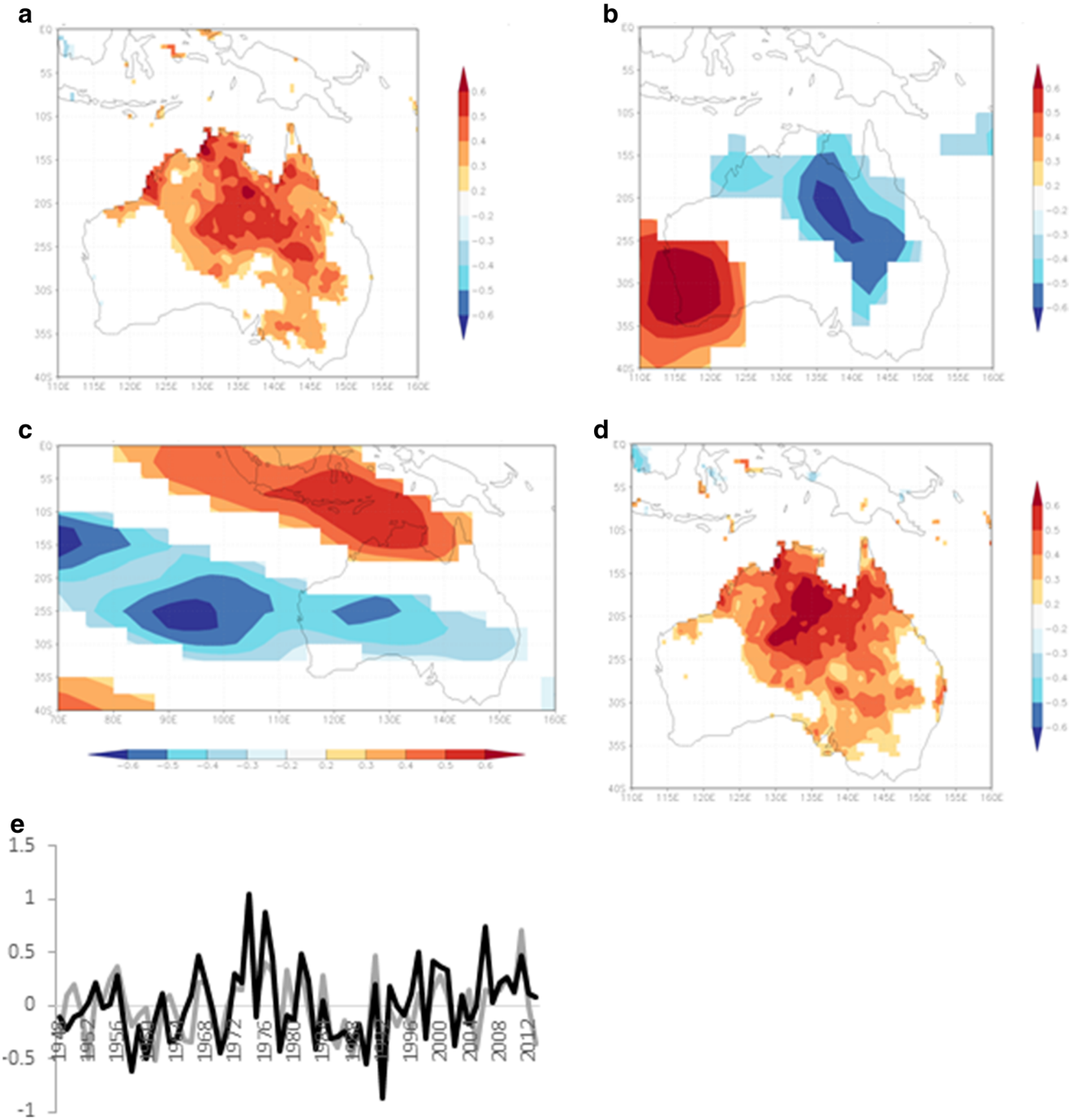

Fig. 8 Correlation between PC2 of 500 hPa geopotential height and **a** precipitation, **b** vertical velocity at 500 hPa and **c** zonal wind at 850 hPa for JFM. **d** Correlation between PC1 of precipitation and an index of 500 hPa geopotential height formed from the difference between that averaged over 125°–132° E 17°–23° S and 60°–80° E 25°–35° S. **e** Time series of this precipitation PC1 (*grey*) and the 500 hPa index (*black*). The two series are correlated at $r = 0.71$ (99.9% significant)

conditions are compounded by increases in maximum temperatures and in the occurrence of more days with temperatures exceeding the 90th percentile over much of Australia (Fig. 7). Thus, variations in the Bilybara High represented by EOF1 can impact strongly on rainfall and temperature characteristics over large parts of Australia.

An even stronger relationship is evident if one correlates an index of 500 hPa geopotential height formed from the difference between that averaged over 110°–115° E 10°–15° S and 50°–60° E 25°–35° S with that of precipitation PC1 (Fig. 6d). This index is motivated by the two regions of highest but opposite signed loadings in the north and southwest of the

domain of the 500 hPa EOF1 that was plotted in Fig. 5a. It essentially measures the pressure gradient between the Bilybara High and the subtropical jet. The resulting 500 hPa index is shown in Fig. 6e (black) along with that of PC1 of precipitation (grey), and these two series are correlated at $r = -0.56$ (99% significant).

For the EOF2 case, the pattern is one in which the High extends substantially onshore and is again located north from its mean position (Fig. 5c). However, in this case, the High is not shifted meridionally as much from its mean position as for EOF1. The zonal wind correlation map (Fig. 8c) is similar to that for EOF1 (Fig. 6c) but opposite in sign. Since the EOF2 pattern is mainly negative whereas EOF1 is mainly positive (Fig. 5), this also implies similar linkages between monsoonal northwesterlies/easterlies and rainfall as above. The spatial correlation with rainfall shows a larger area of significant relationship over tropical Australia and extending into the southeast of the land (Fig. 8a) than is the case for EOF1. This difference in area of the rainfall correlation pattern compared to that shown in Fig. 6a may result because EOF2 shows a much larger area of anomalous uplift over tropical Australia than does EOF1 (Fig. 8b). EOF2 shows a strong negative relationship with maximum surface air temperature over most of central and northern Australia (Fig. 9a) and a slightly weaker and more spatially confined correlation with number of days reaching the 90th percentile of temperature (Fig. 9b). The temperature and rainfall patterns more or less match with those in vertical velocity (Fig. 8b).

Similar to Fig. 6d, e, as discussed above, a stronger precipitation relationship exists between an index of 500 hPa

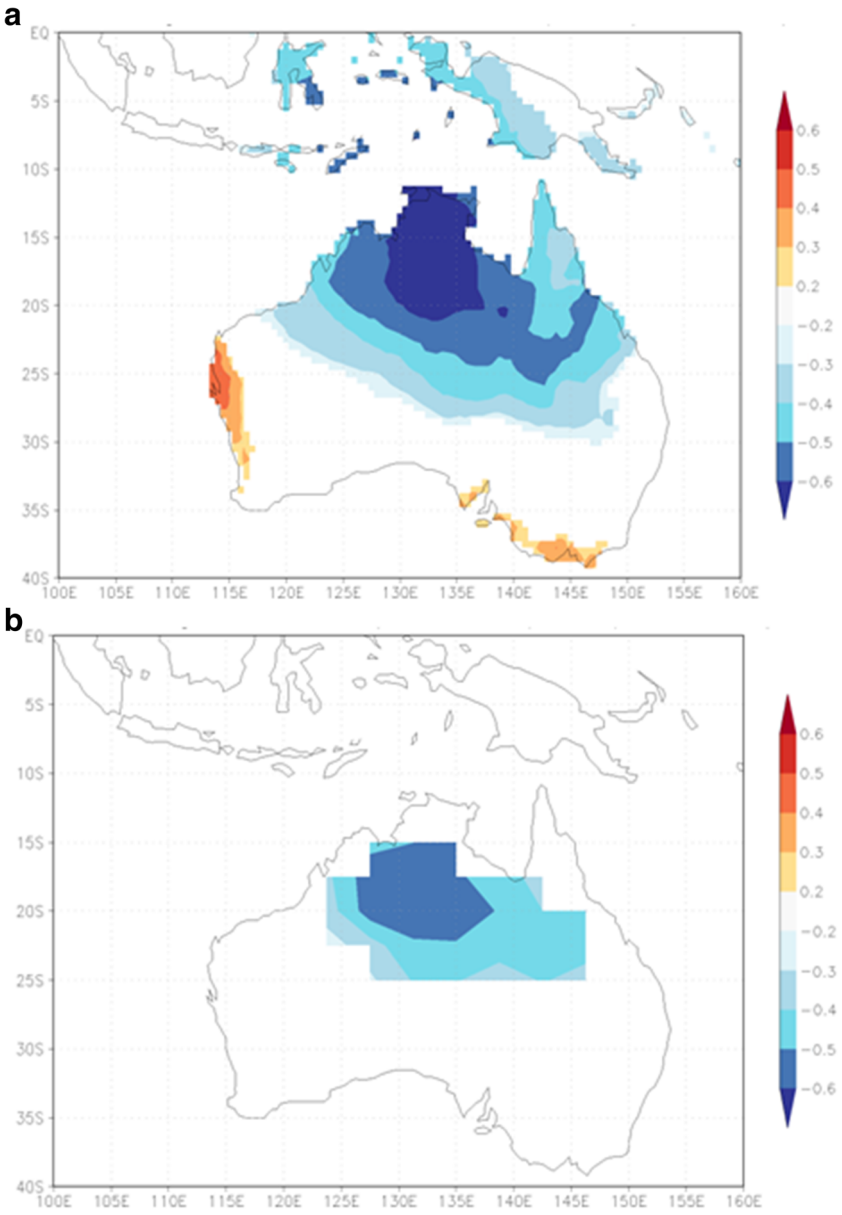

Fig. 9 Correlation between PC2 of 500 hPa geopotential height and **a** maximum surface air temperature and **b** number of days exceeding 90th percentile in surface air temperature for JFM

geopotential height formed from the difference between that averaged over 125°–132° E 17°–23° S and 60°–80° E 25°–35° S (Fig. 8d). In this case, the index is similarly motivated by the regions of highest but opposite signed loadings in Fig. 5c, the EOF2 pattern of 500 hPa height. As before, it essentially measures the pressure gradient between a particular position of the Bilybara High and the subtropical jet to its southwest. Figure 8e shows time series of this precipitation PC1 (grey) and the 500 hPa index (black); these two series are correlated at $r = 0.71$ (99.9% significant).

To further highlight the importance of variations in the Bilybara High for tropical Australian rainfall, Fig. 10a shows a composite of rainfall anomalies for those summers (1967, 1977, 1981, 1991, 1997, 2006, 2009) when the Bilybara High PC2 is strongly positive (i.e. the high is weaker than average) and when there was no ENSO event according to the NOAA CPC Oceanic Niño Index methodology. Two of these years (1967, 1997) also correspond to PC1 being negative and hence also imply a weaker High via this mode. All of tropical Australia shows above average rainfall in the composite of these years together with stronger monsoonal westerlies over the north coastal region and enhanced easterlies further south (Fig. 10b). At 200 hPa, there are enhanced tropical easterlies over the region with stronger upper-level westerlies south of about 30° S (Fig. 10c). The areas of increased rainfall more or less match those with increased uplift in the middle troposphere (Fig. 10d). A composite of neutral summers for which the High was stronger than averaged displays (not shown) more or less the reverse pattern in rainfall and low-level wind.

2.3 Decadal variability

Figures 5, 6, 7, 8, 9, and 10 have presented substantial evidence that interannual variability in tropical Australian rainfall

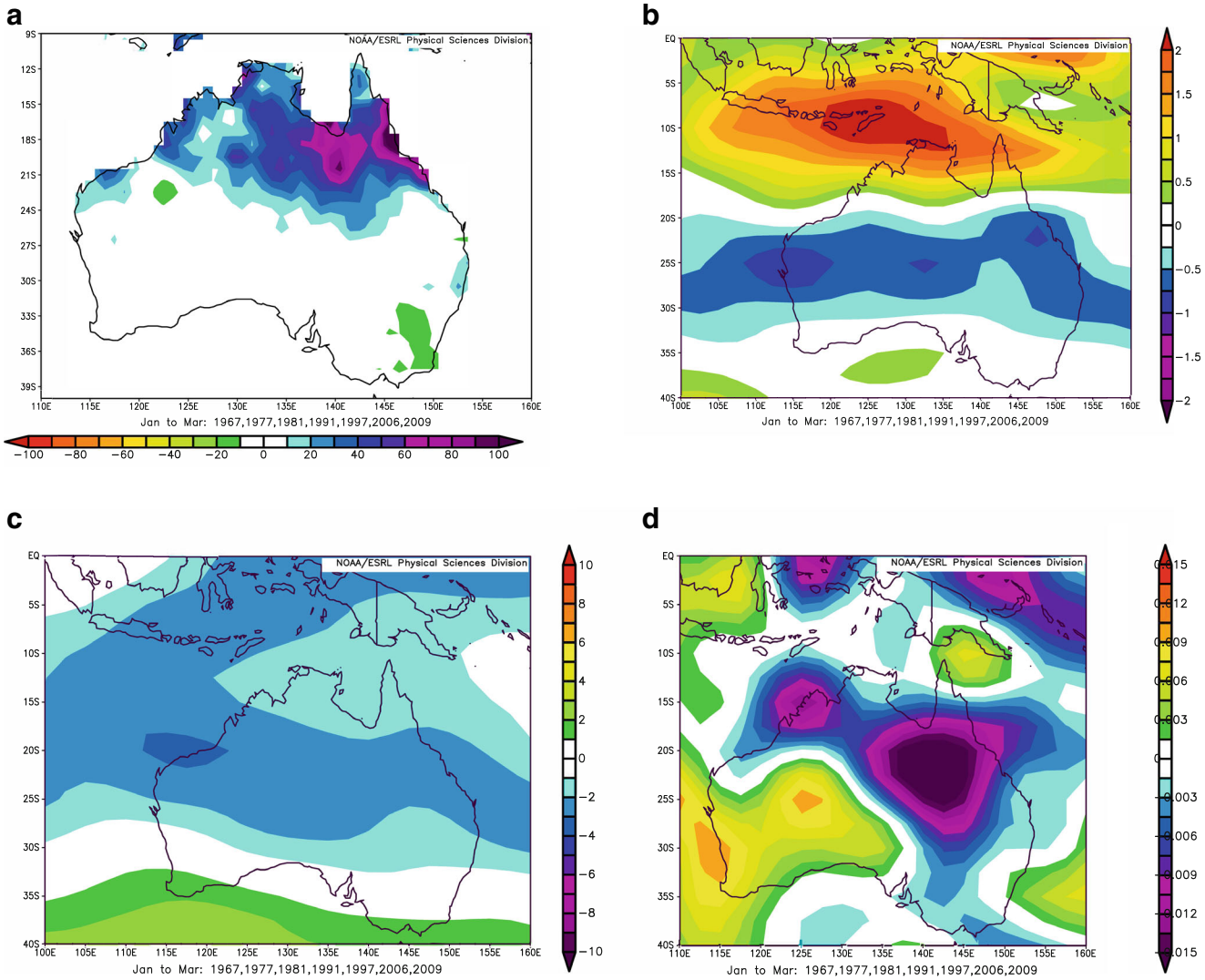

Fig. 10 Composite for neutral summers (1967, 1977, 1981, 1991, 1997, 2006, 2009) of **a** precipitation (mm month^{-1}), **b** zonal wind at 850 hPa (ms^{-1}), **c** zonal wind at 200 hPa (ms^{-1}) and **d** pressure tendency at 500 hPa (Pas^{-1})

during the JFM season is related to changes in the location and strength of the Bilybara High. It is of interest to now consider longer time scales since it has long been known that many parts of Australia experience pronounced interdecadal variability in rainfall. This variability has been linked to several drivers such as the Interdecadal Pacific Oscillation (Power et al. 1999), decadal signals in ENSO (Allan et al. 2003) and to regional changes in atmospheric circulation and blocking (Ansell et al. 2000; Smith et al. 2000; Risbey et al. 2009). Since it roughly corresponds to the data period analysed here, it is worth noting here that Risbey et al. (2009) found a slightly stronger and more spatially extensive correlation between northern Australian summer rainfall and the Southern Oscillation Index for 1948–1976 than for 1977–2005, thus pointing to interdecadal variability in the ENSO-rainfall connection in this part of the country.

Figure 11a, b plots the leading mode of tropical Australian rainfall after the PC has been smoothed with a 7-year running mean together with similarly smoothed PC1 and PC2 of the Bilybara High. The correlation coefficient between the smoothed leading rainfall mode and the Interdecadal Pacific Oscillation is $r = -0.42$ which is a bit stronger than that between the rainfall and the smoothed PC1 of the Bilybara High ($r = -0.34$) (Fig. 11a). A much stronger correlation exists between the smoothed rainfall mode and the smoothed PC2 of the Bilybara High ($r = 0.86$ significant at 99.9%) (Fig. 11b). However, the correlation between the Interdecadal Pacific Oscillation and this smoothed Bilybara High PC2 is close to zero implying that these two modes are unrelated to each other.

Correlating the smoothed rainfall series with 500 hPa geopotential height (Fig. 12a) shows a negative relationship in the region of the Bilybara High together with a strong positive relationship in the Tasman Sea, a region where blocking highs often tend to occur in the Australian region (Risbey et al. 2009). The mechanism again involves changes in the monsoonal northwesterlies towards the northern coast of Australia (Fig. 12b) and in the inflow of moist marine air towards Queensland highlighting the potential importance of variations in the Bilybara High and associated regional circulation. As a result, it seems possible that much of the interdecadal variability in summer rainfall over tropical Australia may be related to either the PC2 pattern in the Bilybara High or the Interdecadal Pacific Oscillation which in turn is related to the PC1 pattern of the Bilybara High.

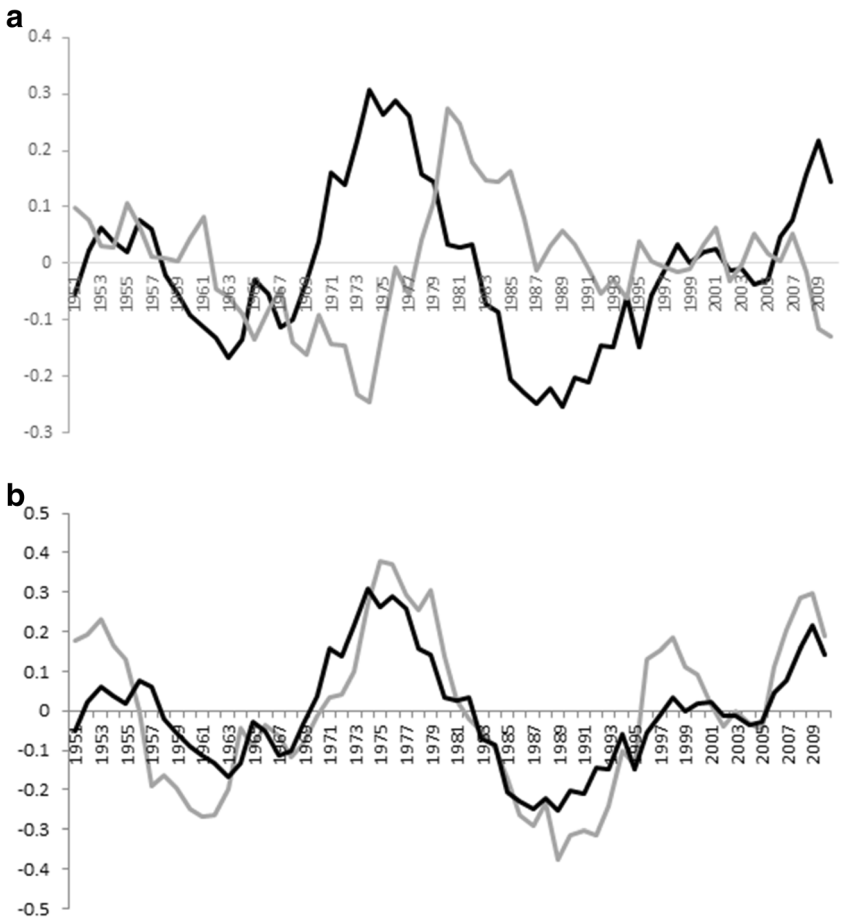

Fig. 11 PC1 of tropical Australian rainfall (*black line*) and **a** PC1 of 500 hPa geopotential height (correlated at $r = -0.34$) and **b** PC2 of 500 hPa geopotential height (correlated at $r = 0.86$) for JFM after all series have been smoothed with a 7-year running mean

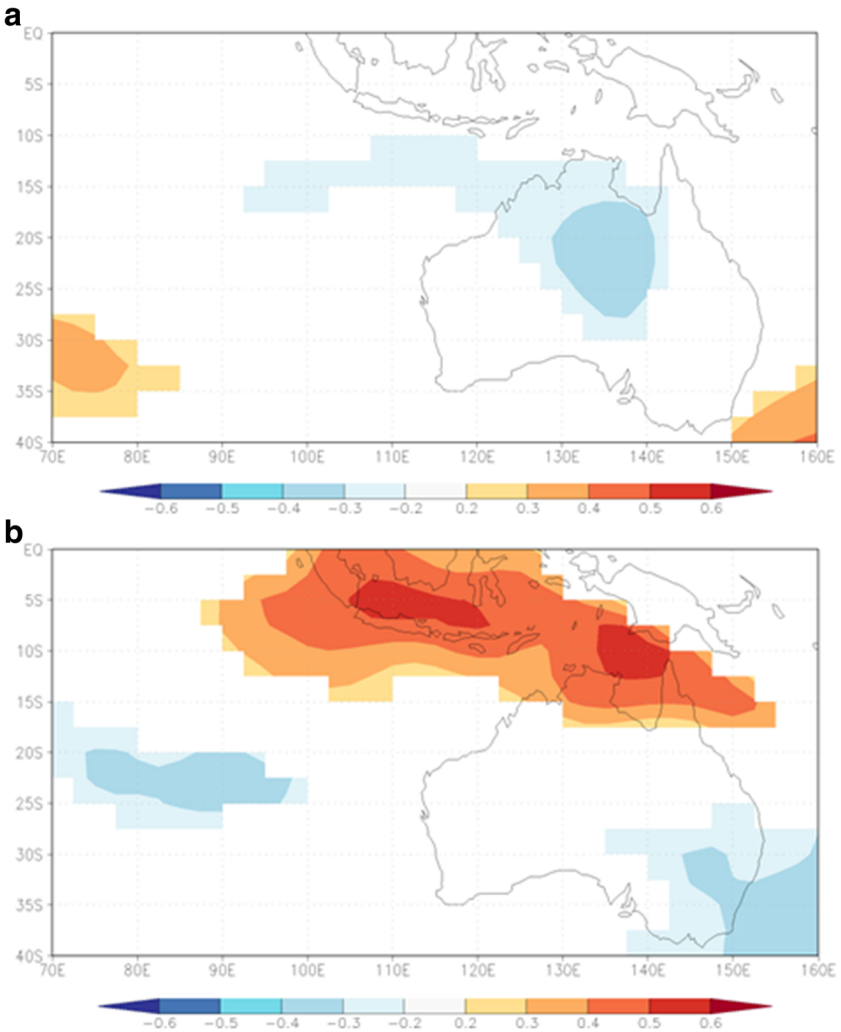

Fig. 12 Correlation between smoothed PC1 of tropical Australian rainfall and **a** 500 hPa geopotential height and **b** 850 hPa zonal wind for JFM

3 Summary and discussion

In this study, EOF analyses have been used to investigate the variability in rainfall over tropical Australia during the summer and its linkages with the mid-level anticyclone (termed the Bilybara High) that occurs over northwestern Australia and the Timor Sea region between about August and April. This regional circulation feature has not been previously studied much despite it being related to regional rainfall and temperature patterns. Typically, the Bilybara High forms in August over the Timor Sea near 12° S and slowly moves south during the spring. This southward movement continues through the early and mid-summer and is accompanied by a substantial increase in its magnitude by January. Like its counterpart in southern Africa, the Botswana High (Reason 2016), the Bilybara High reaches its southernmost extent in February and continues to strengthen. Both anticyclones retreat northwards in March and April, but the Bilybara High does not obviously decrease in strength unlike the Botswana High. In May, neither mid-level anticyclone is clearly evident.

The evolution of the Bilybara High essentially tracks that of the upper-level anticyclone at 200 hPa whose latitudinal position is related to the location in the peak in tropical precipitation and regional monsoon system. Its position is located southwest of this upper-level anticyclone consistent with it forming from a balance between the upper-level divergence over the tropical high precipitation regions and planetary vorticity advection (Lenters and Cook 1997).

Variations in the position and strength of the Bilybara High were shown to be linked with summer rainfall and temperature patterns over large areas of tropical Australia as well as parts of southern Australia. The mechanisms involve modulations in the low-level monsoonal northwesterly flow from the eastern equatorial Indian Ocean/Timor Sea region towards northern Australia and, further south, in the easterly trade winds. Some of these variations in the High are related to ENSO, but there are also a number of neutral years when such changes in the High impact on regional precipitation and temperature. On decadal time scales, there is a strong relationship between the leading mode of tropical Australian precipitation and the Bilybara High.

Therefore, the results suggest that better understanding the variability in the Bilybara High position and strength could be useful for rainfall and temperature climate impact assessments over Australia and for regional climate prediction efforts.

Acknowledgements NOAA (http://www.esrl.noaa.gov) and the KNMI (http://climexp.knmi.nl) are thanked for providing the freely accessible online data and plotting tools used in this study.

References

Allan RJ, Reason CJC, Lindesay JA, Ansell TJ (2003) Protracted ENSO episodes over the Indian Ocean region. Deep-Sea Res. II, Special Issue on Physical Oceanography of the Indian Ocean: From WOCE to CLIVAR 50:2331–2347

Ansell TJ, Reason CJC, Smith IN, Keay K (2000) Evidence for decadal variability in southern Australian rainfall and relationships with regional pressure and sea surface temperature. Int J Climatol 20:1113–1129

Behera SK, Yamagata T (2001) Subtropical SST dipole events in the southern Indian Ocean. Geophys Res Lett 28:327–330

Cook GD, Heerdegen RG (2001) Spatial variation in the duration of the rainy season in monsoonal Australia. Int J Climatol 21:1723–1732

Davidson NE, McBride JL, McAvaney BJ (1983) The onset of the Australian monsoon during winter MONEX: synoptic aspects. Mon Weather Rev 111:496–516. doi:10.1175/1520-0493(1983)1112.0.CO;2

Drosdowsky W (1996) Variability of the Australian summer monsoon at Darwin: 1957–92. J Clim 9:85–96

Feng M,McPhaden MJ,Xie S-P,Hafner J (2013) La Niña forced unprecedented Leeuwin Current WARMING IN 2011.Sci R 3:1277

Godfred-Spenning C, Reason CJC (2002) Variability of lower tropospheric moisture transport during the Australian monsoon. Int J Climatol 22:509–532

Kalnay E, co-authors (1996) The NCEP/NCAR 40-year reanalysis project. Bull Amer Meteor Soc 77:437–471

Kataoka T, Tozuka T, Behera S, Toshio Yamagata (2014) On the Ningaloo Niño/Niña. Clim Dynam 43 (5-6):1463-1482

Lenters JD, Cook KH (1997) On the origin of the Bolivian High and related circulation features of the South American climate. J Atmos Sci 54:656–677

Leslie LM (1980) Numerical modelling of the summer heat low over Australia. J Appl Meteorol 19:381–387. doi:10.1175/1520-0450(1980)0192.0.CO;2

Power S, Casey T, Folland C, Colman A, Mehta V (1999) Inter-decadal modulation of the impact of ENSO on Australia. Climate Dyn 15: 319–324

Reason CJC (2016) The Bolivian, Botswana and Bilybara Highs and Southern Hemisphere drought/floods. Geophys Res Lett 43:1280–1286. doi:10.1002/2015GL067228

Risbey JS, Pook MJ, McIntosh PC, Wheeler MC, Hendon HH (2009) On the remote drivers of rainfall variability in Australia. Mon. Wea. Rev. 137:3233–3253

Ropelewski CF (1989) Precipitation patterns associated with high index phase of Southern Oscillation. J Clim 2:268–284

Ropelewski CF, Halpert MS (1987) Global and regional scale precipitation patterns associated with El Niño/Southern Oscillation. Mon Wea Rev 115:1606–1626

Schneider U, Fuchs T, Meyer-Christoffer A, and B. Rudolf (2008) Global precipitation analysis products of the GPCC. Global Precipitation Climatology Centre (GPCC), Deutscher Wetterdienst. Available online at; ftp://ftp-anon.dwd.de/pub/data/gpcc/PDF/GPCC_intro_products_2008.pdf

Smith TM, Reynolds RW (2004) Improved extended reconstruction of SST (1854-1997). J Clim 17:2466–2477

Smith IN, McIntosh P, Ansell TJ, Reason CJC, McInnes KL (2000) South-west Western Australian winter rainfall and its association with Indian Ocean climate variability. Int J Climatol 20:1913–1930

Suppiah R, Hennessy KJ (1996) Trends in the intensity and frequency of heavy rainfall in tropical Australia and links with the Southern Oscillation. Aust Meteor Mag 45:1–17

Tozuka T, Kataoka T, Yamagata T (2014) Locally and remotely forced atmospheric circulation anomalies of Ningaloo Niño/Niña. Clim Dynam 43 (7-8):2197-2205